THE PROTEIN SOCIETY

Protein dynamics and the all-ferrous $[Fe_4S_4]$ cluster in the nitrogenase iron protein

Ming-Liang Tan,[1] B. Scott Perrin Jr.,[2] Shuqiang Niu,[1] Qi Huang,[1] and Toshiko Ichiye[1,2]*

[1]Department of Chemistry, Georgetown University, Washington, District of Columbia 20057
[2]Laboratory of Computational Biology, National Heart, Lung and Blood Institute, National Institutes of Health, Bethesda, Maryland 20892

Received 5 May 2015; Accepted 12 August 2015
DOI: 10.1002/pro.2772
Published online 14 August 2015 proteinscience.org

Abstract: In nitrogen fixation by *Azotobacter vinelandii* nitrogenase, the iron protein (FeP) binds to and subsequently transfers electrons to the molybdenum–FeP, which contains the nitrogen fixation site, along with hydrolysis of two ATPs. However, the nature of the reduced state cluster is not completely clear. While reduced FeP is generally thought to contain an $[Fe_4S_4]^{1+}$ cluster, evidence also exists for an all-ferrous $[Fe_4S_4]^0$ cluster. Since the former indicates a single electron is transferred per two ATPs hydrolyzed while the latter indicates two electrons could be transferred per two ATPs hydrolyzed, an all-ferrous $[Fe_4S_4]^0$ cluster in FeP is potenially two times more efficient. However, the 1+/0 reduction potential has been measured in the protein at both 460 and 790 mV, causing the biological significance to be questioned. Here, "density functional theory plus Poisson Boltzmann" calculations show that cluster movement relative to the protein surface observed in the crystal structures could account for both measured values. In addition, elastic network mode analysis indicates that such movement occurs in low frequency vibrations of the protein, implying protein dynamics might lead to variations in reduction potential. Furthermore, the different reductants used in the conflicting measurements of the reduction potential could be differentially affecting the protein dynamics. Moreover, even if the all-ferrous cluster is not the biologically relevant cluster, mutagenesis to stabilize the conformation with the more exposed cluster may be useful for bioengineering more efficient enzymes.

Keywords: reduction potentials; elastic network mode analysis; metalloprotein; iron–sulfur proteins

Introduction

The nitrogenases, which reduce atmospheric nitrogen in bacteria, are the major source of biological nitrogen fixation. In *Azotobacter vinelandii* nitrogenase, iron proteins (FeP) bind to the molybdenum–iron protein (MoFeP) to catalyze the reaction.[1] The catalytically active form of FeP contains a reduced $[Fe_4S_4]$ cluster and two bound MgATPs; upon binding to MoFeP, electrons are transferred from the cluster to MoFeP and the ATPs are hydrolyzed. In MoFeP, the electrons are accepted by the P-cluster, which contains the $[Fe_8S_7]$ core, and then transferred to the FeMoco, which contains the $[MoFe_7S_9]$-homocitrate site, where reduction of N_2 is thought to occur.

The redox state of the reduced cluster has been debated for 20 years, although the prevailing view is that one electron is transferred from a $[Fe_4S_4]^{1+}$ cluster in FeP via the $[Fe_4S_4]^{2+}/[Fe_4S_4]^{1+}$ couple. Initially, the

Grant sponsor: National Institutes of Health; Grant number: GM045303.

*Correspondence to: Toshiko Ichiye; Department of Chemistry, Georgetown University, Washington, DC, 20057.
E-mail: ti9@georgetown.edu

discovery of an all-ferrous $[Fe_4S_4]^0$ in FeP with a reduction potential for the $[Fe_4S_4]^{1+}/[Fe_4S_4]^0$ couple of E° = 460 mV using methyl viologen[2] sparked interest because two electrons could be transferred per two ATPs via the $[Fe_4S_4]^{2+}/[Fe_4S_4]^0$ couple, thus increasing the overall energy efficiency.[3] Later measurements using Ti(III) citrate found that the reduction to $[Fe_4S_4]^0$ with an $S = 4$ spin state by Mössbauer and electron paramagnetic resonance (EPR)[4] occurs at E° = 790 mV,[5] which is outside of the physiological range and thus indicated that the all ferrous form is not relevant to the nitrogenase reaction. In addition, calculations of FeP using density functional theory (DFT) and Poisson–Boltzmann (PB) continuum electrostatic calculations supported the latter value.[6] However, more recent EPR studies indicate that flavodoxin hydroquinone (FldHQ), a physiological reductant of FeP, reduces FeP to $[Fe_4S_4]^0$ with $S = 0$ near E° = 460 mV,[7] in support of the higher value of E°. Other studies have measured the Ti(IV)/Ti(III) couple at E° = 510 mV,[8] which also leads to questions about the lower value of E°. On the other hand, recent Mössbauer, EPR, and DFT studies of an analog in the gas phase indicate that $[Fe_4S_4]^0$ is not $S = 0$ but $S = 4$,[9,10] in support of the lower value of E°. However, since the earlier DFT calculations indicate that the $S = 0$ state of an analog in the gas phase is actually slightly lower in energy than the $S = 4$ state,[6] it appears likely that either could be stabilized in the protein given the experimental evidence that both $S = 0$ and $S = 4$ states are found in the protein for $[Fe_4S_4]^0$. Moreover, the real question is whether the all-ferrous cluster in FeP can be reached under physiological conditions, regardless of spin state. Interestingly, it has been shown that two electron reduction by $[Fe_4S_4]^0$–FeP of MoFeP occurs at the same rate as two one electron reductions by $[Fe_4S_4]^{1+}$–FeP,[7] and more recently, that the interconversion from $2[Fe_4S_4]^{1+}$–FeP $\rightarrow [Fe_4S_4]^{2+}$–FeP + $[Fe_4S_4]^0$–FeP does not appear to be a source of $[Fe_4S_4]^0$,[11] so that the question of one electron reduction of $[Fe_4S_4]^{1+}$–FeP under physiological conditions becomes even more relevant.

Nitrogenase is a protein complex that has been characterized very well structurally.[3] Crystal structures of FeP (α_2, M_r = 64 kda) in various combinations of nucleotide binding and of complexation with MoFe ($\alpha_2\beta_2$, M_r = 230 kda) have been solved. These studies have led to proposals that solvent exposure of the cluster may play a role in making the all-ferrous cluster accessible.[12] Interestingly, the cluster moves ~5 to 8 Å closer to the surface of FeP bound by MgATP analogs when in complex with MoFeP, which brings the $[Fe_4S_4]$ cluster within a reasonable electron transfer distance of the P-cluster.[13] The cluster movement appears to be stabilized by MgATP and not complexation with MoFe since only complexes with analogs with two MgATPs, or most recently, with one MgATP and one MgADP,[14] show movement of the cluster towards the FeP surface but not the nucleotide-free or MgADP bound complexes.[13] Unfortunately, the only crystal structures for FeP with MgATP analogs bound are also in complex with MoFeP. In addition, calculations using the DFT+PB method show that the burial of a cluster is important in determining E°.[15] Since many other enzymes in their unbound form are thought to exhibit low frequency motions in solution between conformations corresponding to free and complexed forms found in crystal structures,[16] this leads to the question of whether the 300 mV variation in observed E° for FeP can be attributed to a low frequency motion of the protein in which the entire cluster moves relative to the protein surface. Such a protein motion could make the all-ferrous state at least transiently accessible under biological conditions. Moreover, even if it is not transiently accessible under biological conditions, site-specific mutagenesis to stabilize the conformation with the more exposed cluster may be useful for bioengineering a more efficient enzyme.

The DFT+PB method has been shown to give good reduction potentials of iron–sulfur proteins in comparison to experimental measurements.[15,17,18] In DFT+PB, the reduction energy of the iron–sulfur redox site is calculated using highly benchmarked DFT methods, in which the functionals and basis sets were chosen based on excellent agreement with electron detachment energies of multiple iron–sulfur analogs and other iron compounds measured by electrospray photoelectron spectroscopy.[19] The protein response to the reduction of the redox site is calculated from the interaction of the protein environment, which is treated as an electrostatic continuum, with a partial charge representation of the redox site, where the partial charges were also from DFT calculations with the same functionals and basis sets.[20]

Here, the causes of the 300 mV variation in the reported E° of the $[Fe_4S_4]^{1+}/[Fe_4S_4]^0$ couple for FeP are explored via DFT+PB calculations of FeP using different crystal structures. In particular, we seek to determine ways that the all-ferrous form could occur *in vivo*. In addition, the vibrational modes of FeP in different binding states are calculated using elastic network mode (ENM) analysis.[21]

Methods

To study E° computationally, the total E° versus the standard hydrogen electrode (SHE) must be determined, not just a relative value. The total E° can be decomposed as

$$-nFE^\circ = \Delta G^\circ \approx \Delta G_{in} + \Delta G_{out} + \Delta G_{SHE} \qquad (1)$$

where n is the number of electrons transferred, F is the Faraday constant, ΔG_{in} and ΔG_{out} are the inner and outer sphere free energies of reduction, respectively, and $\Delta G_{SHE}/F = 4.43$ eV[22] is the absolute electrode potential for the SHE. In the DFT+PB approach, ΔG_{in}

Table I. *Partial Charges (in e) for [4Fe4S(SCH$_2$)$_4$]^n*

Atom	$n = -2$	$n = -3$	$n = -4/S = 0$	$n = -4/S = 4$
Fe	0.733	0.842	0.915	0.906
S	−0.668	−0.856	−1.045	−1.036
Sγ	−0.693	−0.839	−0.956	−0.950
C_β	−0.052	−0.077	−0.094	−0.100
H_β	0.090	0.090	0.090	0.090

is the difference in free energy calculated using DFT between an oxidized and reduced redox site analog in the gas phase and ΔG_{out} is the difference in the interaction energy calculated using PB of the partial charges from DFT of the oxidized and reduced redox site with the surrounding protein and solvent.[20]

The ΔG_{in} and partial charges of $[Fe_4S_4(SCH_3)_4]^n$ (n = 2-, 3-, 4-) are from BS-DFT calculations using the NWChem program package[23] with the B3LYP exchange-correlation functional[24,25] as previously described.[19,20] Briefly, the geometries of each redox state were optimized using the 6-31G**[26] basis sets and the vibrational analysis for the free energies and CHELPG[27] electrostatic potential (ESP) charges were calculated at the level of the geometry optimization. Single point energies with added *sp*-type diffuse functions into the 6-31G** basis set on the sulfurs were calculated from the 6-31G** geometries. ΔG_{in} were calculated as SCF energy differences of the optimized oxidized and reduced states, with additional terms for the free energy from vibrational analysis. Partial charges (Table I) from our DFT calculations using previous described methods[19] were used for the $[Fe_4S_4]$ redox sites; however, since it was not possible to determine the redox layers from the crystal structures, all irons were assumed to be equivalent, all inorganic sulfurs were assumed to be equivalent, all cysteinyl sulfurs were assumed to be equivalent, and all carbons were assumed to be equivalent. In addition, all hydrogen atoms were assigned a charge of 0.09 e and the charge on the carbon to which they were attached was assigned a charge such that the net charge on the entire methyl group was maintained. Calculations assigning layers did not show significant differences.

Crystal structures of *Azotobacter vinelandii* (*Av*) FeP at 2.25 Å resolution [Protein Data Bank (PDB) ID: 1G5P],[12] bound to MgADP at 3.15 Å resolution [PDB ID: 1FP6],[28] and bound to MgAMPPCP and the MoFe protein at 2.30 Å resolution [PDB ID: 2AFK],[13] and of *Clostridium acidurici* (Ca) ferredoxin at 0.94 Å resolution [PDB ID: 2FDN][29] were obtained from the PDB.[30] Since coordinates were missing for 1G5P and two copies of FeP are in the asymmetric unit, missing heavy atoms were added from the complementary chain. Since even more coordinates were missing for 2AFK from CHARMM22 parameters and four copies of FeP are in the asymmetric unit, missing heavy atoms were first added from the complementary chain and then from the 1GFP structure. In addition, the ATP analogue MgAMPPCP in 2AFK was used as a template to build the MgATP. No coordinates were missing for 1FP6. Also, hydrogen atom positions were added with HBUILD in CHARMM[31] version 35b1.

All solvation energies and electrostatic potentials were calculated using APBS,[32] a program for solving the Poisson–Boltzmann equation, as described fully elsewhere[22] and summarized briefly here. Radii for Connolly surfaces[33] of the proteins and redox sites and partial charges for the protein were from the CHARMM22 parameters.[34] The dielectric permittivity were chosen as $\varepsilon_c = 1$, $\varepsilon_p = 4$, and $\varepsilon_w = 78$ and the ionic concentration was set to zero. A 76.8 Å × 76.8 Å × 76.8 Å box with 385 grid points in each direction was used, at a constant 0.2 Å spacing for all proteins. The redox site was defined to include all metal ligands up to the C_β for side chains of the protein.

Elastic network model analyses[21,35] were carried out on the AD-ENM Web Server. To represent the cofactors, CA were added to each heavy atom since springs are only included between CA and additional dummy atoms were added to mimic the heavier atoms. Specifically, in the [4Fe–4S] cluster, Fe was represented by CA + O + CB + C and S by CA + CB + C and, in the Mg–ADP/ATP, Mg was represented by CA + CB, O by CA, N by CA, and P by CA + O. To convert the ENM frequency to cm^{-1}, a residue–residue force constant of 0.1 kcal/mol-Å^2 and a residue mass of ∼100 g/mole were assumed. The overlaps of the modes with different reference structures were also calculated and reported as a value between 0 and 1, with 1 indicating maximum overlap. The modes were numbered from the lowest nonzero frequency, and the conformations obtained by adding or subtracting the eigenvector were labeled as ± to denote the one closer to/away from the reference crystal structure. Since only coordinates for the backbone are generated, approximate coordinates of the side chains were generated for the radius of gyration and R_p calculations from the crystal structures. The crystal structure and the ENM structure were first divided into 20 fragments each. Next, every fragment of the crystal structure was aligned to the corresponding fragment of the ENM structure and

Table II. *Inner Sphere Reduction Energy for [4Fe–4S] with "S4" Symmetry*

Initial charge	Initial spin	Final charge	Final spin	ΔG_{in} (eV)
2+	0	1+	1/2	3.452
1+	1/2	1+[a]	7/2	0.193
1+	1/2	0	0	6.669
1+	1/2	0[a]	4	6.794

[a] Has one negative frequency so uses frequencies from the same oxidization state and the lowest spin state without negative frequencies.

Table III. *Calculated and Experimental Reduction Potentials (E°) in mV for Iron Protein (FeP) and Ferredoxin (Fd), for Different Couples and Spin States*

Protein (PDB ID)	Couple	$E°_{cal}$	$E°_{exp}$
FeP (1G5P)	2+/1+	−315	−300
Fd (2FDN)	2+/1+	−373	−430
FeP* (2AFK)	1+/0, S = 0	−347	−460
FeP* (2AFK)	1+/0, S = 4	−508	NA
FeP*-MgATP (2AFK)	1+/0, S = 0	−517	$E°$(FeP*–MgATP) < $E°$(FeP)
FeP*-MgATP (2AFK)	1+/0, S = 4	−678	NA
FeP-MgADP (1FP6)	1+/0, S = 0	−561	$E°$(FeP–MgADP) < $E°$(FeP*–MgATP)
FeP-MgADP (1FP6)	1+/0, S = 4	−686	NA
FeP (1G5P)	1+/0, S = 0	−640	NA
FeP (1G5P)	1+/0, S = 4	−765	−790
Fd (2FDN)	1+/0, S = 0	−741	NA
Fd (2FDN)	1+/0, S = 4	−901	NA

the side chain coordinates from the crystal structure were added to the ENM structure.

Results and Discussion

The results of the DFT+PB are presented first, followed by the ENM analysis. For ease of discussion, the $[Fe_4S_4]^m/[Fe_4S_4]^n$ couples will be referred to as *m/n* couples, with the spin state included if necessary.

Examining the inner sphere contribution first, our DFT calculations (Table II) show that ΔG_{in} = 3.45 eV for the 2+/1+ couple, while ΔG_{in} = 6.67 and 6.79 eV for the 1+/0 couple where $S = 0$ and $S = 4$ in the reduced state, respectively. As in earlier works,[6] $S = 0$ state is very slightly lower than $S = 4$ state in energy for the analog in vacuum by ~3 kcal/mol, although we were unable to find an absolute minimum for the $S = 4$ state (that reported in Table II had one negative frequency) because the potential is very flat. Although this is in disagreement with the experimental observation that the ground state of analog in vacuum the $S = 4$ state,[9,10] our other calculations indicate that the $S = 4$ state may be the observed state because it is kinetically trapped. Moreover, the difference in ΔG_{in} of only ~120 meV for the 1+/0 couple between $S = 0$ and 4 is not large enough to account for the difference between the experimental $E°$ for FeP at −460 and −790 mV.

Examining the entire protein next, our DFT+PB calculations of $E°$ for FeP from the cystal structure of the uncomplexed protein without nucleotide (1G5P) are shown in comparison to those for ferredoxin (Fd), which is a small, 55-residue protein with two $[Fe_4S_4]$ clusters (Table III). The $E°$ for the 2+/1+ couple predicted for FeP and Fd are in reasonable agreement with experiment.[36,37] In addition, the $E°$ for the 1+/0, $S = 4$ couple predicted for FeP is close to the experimental $E° = -790$ mV for reduction by Ti(III) citrate. Thus it is out of the *in vivo* range, in agreement with previous calculations.[6] In addition, the $E°$ for the 1+/0, $S = 4$ couple predicted for Fd is out of the *in vivo* range and is not observed experimentally. Interestingly, the $E°$ for the 1+/0 couple with *either spin* for the all-ferrous state predicted for FeP* are within the *in vivo* range, similar to the experimental $E° = -460$ mV using methyl viologen. The coordinates for FeP* are from the crystal structure of the MoFeP:FeP complex with bound MgAMPPCP (2AFK), an MgATP analog,[13] except the coordinates of MgAMPPCP and MoFeP are excluded in the calculation. Calculations using the other crystal structures with native *A. vinelandii* FeP in the PDB are also consistent; that is, only the other structure from a complex with MoFeP with another MgATP analog bound has a predicted $E°$ near −460 mV (if the coordinates of MoFeP and MgATP analog are excluded) while the rest of the structures give values close to −790 mV.

The effects of nucleotide binding to FeP were also examined (Table III). The predicted value of $E°$ for the 1+/0 couple for FeP*–MgATP (2AFK), which is also from the same structure as FeP* except now an MgATP is built into the coordinates from the MgAMPPCP and only the coordinates of MoFeP are excluded, is barely within the physiological range, and that for FeP–MgADP is even more negative by a slight amount. This is consistent with the experimental observation that

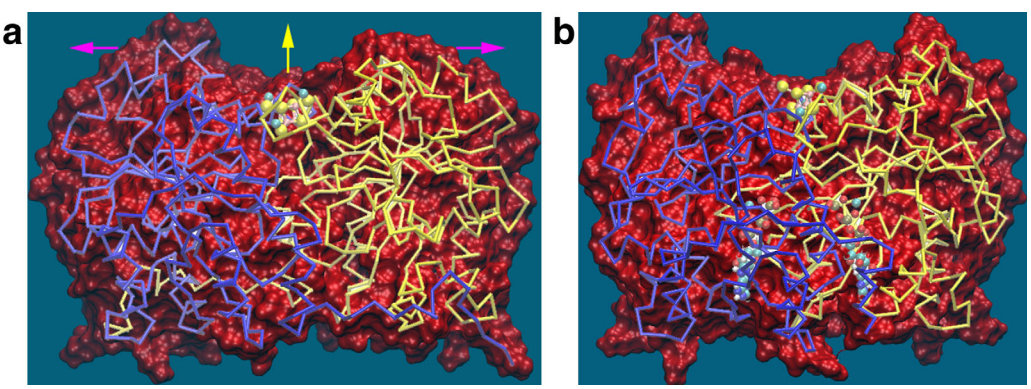

Figure 1. Structures of (a) uncomplexed FeP (1G5P) and (b) FeP with MgATP analog bound (2AFK) with the solvent accessible surface (red), the protein backbone (blue and yellow), cluster (yellow, pink, and green balls), and two MgATP (light blue, dark blue, and red balls). Mode 1 is indicated by magenta arrows and Mode 2 by yellow arrows.

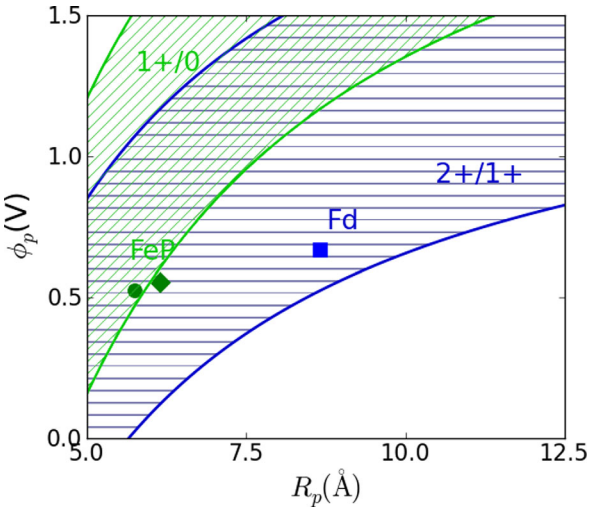

Figure 2. R_p vs φ_p for FeP* (green circle), uncomplexed FeP (green diamond), FeP-MgADP (green cross), and CaFd (blue square). The shaded area indicates the R_p and φ_p that give E^o between −0.5 V and 0.5 V with $\Delta G_{in} = 3.45$ eV (blue lines) for the 2+/1+ couple and $\Delta G_{in} = 6.67$ eV (green lines) for the 1+/0 couple.

FldHQ rapidly reduces ~73% of $[Fe_4S_4]^{1+}$ FeP bound by MgATP and ~40% of $[Fe_4S_4]^{1+}$ FeP bound by MgADP to the $[Fe_4S_4]^0$ state.[7] Note that the conformations in which the cluster is close to the surface for FeP*–MgATP but buried for FeP–MgADP could explain why the FeP–MgATP is actually higher in potential even though it is bound by a more negatively charged co-factor if MgATP stabilizes the FeP* conformation. This is also consistent with the observations for the 2+/1+ reduction potentials for the nucleotide bound states.[1] In addition, it explains why the ATP bound form is necessary for the reduction.

The predicted E° of FeP* is higher than FeP (and Fd) apparently because the cluster is closer to the surface of the protein (Fig. 1). To quantitate this observation, the dielectric radius R_p, a measure of cluster burial, and the electret potential ϕ_p, the average electrostatic potential at the redox site,[18] are calculated for each protein, along with the biological ranges of R_p and ϕ_p for the 2+/1+ and 1+/0 couples (Fig. 2). R_p becomes more important in determining E° with increasing magnitude of Q, the net charge of the entire redox site (i.e., $[Fe_4S_4Cys_4]$; for the all-ferrous form, $Q = -4$). Since the outer sphere contribution is a function of Q, the net charge of the entire redox site including the metals and the ligands and can be estimated by

$$\Delta G_{out} \approx -Q^2\left[\frac{1}{2R_c}\left(1-\frac{1}{\varepsilon_p}\right)+\frac{1}{2R_p}\left(\frac{1}{\varepsilon_p}-\frac{1}{\varepsilon_w}\right)\right]+Q\phi_p \quad (2)$$

where R_c is the Born radius of the cluster.[18] All three structures indicate the proteins are in the range of the 2+/1+ couple while only FeP* also falls in range of the 1+/0 couple because, even though ϕ_p is almost the same, which indicates the polarization around the redox sites is similar, R_p is smaller, which indicates the redox site is closer to the surface in FeP*. Interestingly, R_p for FeP–MgATP is even smaller than FeP, indicating that it is more buried, which is also consistent with the results in Table III.

The cluster movement seen in FeP* suggests that the uncomplexed FeP in solution may have a low frequency motion or conformational transition that also moves the entire cluster. Thus, an ENM analysis[21] of FeP was performed (Table IV). The lowest nonzero frequency mode is a twisting motion and the second lowest is a hinge bending motion. They both correspond to motion of the entire cluster relative to surface (yellow arrows in Fig. 1); in addition, both also correspond to opening of the top (magenta arrows in Fig. 1). Moreover, the high overlap of these modes with the FeP* structure (Table IV) indicates that uncomplexed FeP exhibits low frequency motions between the conformations in the crystal structures of uncomplexed FeP (Fig. 1a) and FeP* (Fig. 1b). In these modes, the conformation resulting from adding or subtracting the eigenvector that brings it closer to FeP* also has the smaller R_p, just as FeP* has a smaller R_p than FeP (Table IV); note that the changes in R_p obtained from the ENM conformations are expected to be smaller since the modes are calculated with the harmonic approximation and these low frequency modes are likely to be highly anharmonic. Interestingly, the two lowest modes of FeP–MgADP (Table IV) are similar to those of FeP but at about twice the frequency so that they are harder to excite. The high overlap of these modes with the FeP*–MgATP structure (Table IV) indicates that FeP–MgADP exhibits low frequency motions between the conformations in the crystal structures of FeP–MgADP and FeP*–MgATP. In these modes, the conformation resulting from adding or subtracting the eigenvector that brings it closer to FeP* also has the smaller R_p, just as FeP* has a smaller R_p than FeP (Table IV).

The calculations here do not establish the spin state of the all-ferrous cluster in FeP, since the $S = 4$

Table IV. *ENM Analysis of FeP, with Frequency, Overlap with Reference Structure (2AFK), and Effective Radius*

Structure	Mode	Frequency (cm^{-1})	Overlap with reference	R_p of ± (Å)[a]
FeP/FeP[a]	(Crystal)			6.14/5.74
	1	0.092	0.38	6.15/6.02
	2	0.131	0.60	6.22/6.14
FeP-MgADP/	(Crystal)			6.45/5.74
FeP[a]–MgATP	1	0.163	0.32	6.48/6.41
	2	0.251	0.23	6.61/6.28

[a] For (crystal), the two radii are for the two crystal structures of pair; for the modes, the two radii are for the – and + conformations (see methods).

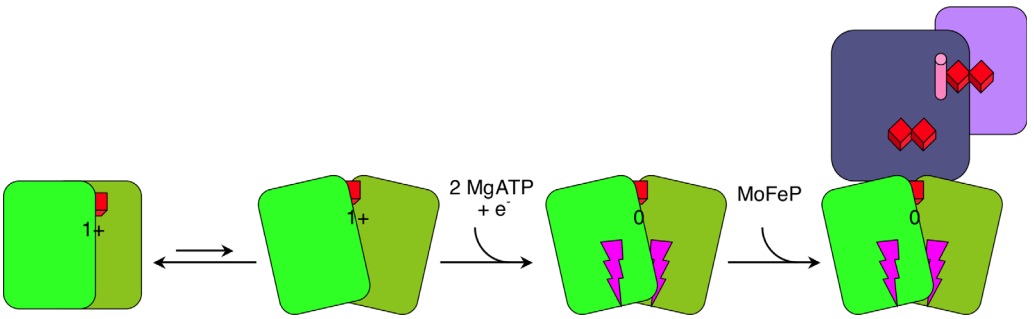

Figure 3. Schematic of interactions of Fe protein and MoFe protein. An Fe protein dimer is shown in green and one half of the MoFe protein (an αβ-unit) is shown in purple. The [Fe4S4] cluster is a red cube labeled with the redox state, the P-cluster is two fused red cubes, the FeMo-cofactor is shown as two fused cubes with a pink cylinder, and the MgATP are shown as magneta lightening bolts.

state of the cluster is only ~3 kcal/mole higher in energy than in the $S = 0$ state, which could easily be compensated by small changes in the protein. Instead, these results indicate that FeP fluctuates between two protein conformations in which the cluster is alternatively more buried and more exposed (Fig. 3, left two structures), with the equilibrium most likely towards the left since the 1G5P crystal structure of isolated FeP has the buried cluster. This equilibrium could easily be shifted under different experimental conditions such as different reductants. However, even under normal conditions FeP would occasionally be in the more exposed cluster conformation. If two MgATP bind first to FeP in this conformation, presumably the more stable MgATP binding mode based on the 2AFK crystal structure and because the negatively charged MgATP are further from the negatively charged $[Fe_4S_4Cys_4]^{3-}$ redox site, the cluster would be more readily reduced to the all-ferrous form. On the other hand, if an electron first reduced the cluster to the all-ferrous form while FeP was in the exposed cluster conformation, fluctuation back to the buried cluster conformation could trap the electron until two MgATP could bind since the cluster would be much farther from the surface. Once both the two MgATP bound and the cluster was in the all-ferrous form (Fig. 3, third structure), FeP in the exposed cluster conformation would be stabilized and would bind readily to MoFeP (Fig. 3, right most structure). Of course, this does not rule out alternative pathways and more than one pathway could operate; however, this does suggest that the all-ferrous form may have importance in the nitrogenase reaction.

Conclusions

The movement of cluster due to protein conformational dynamics based on the crystal structures and the ENM analysis can rationalize how the $[Fe_4S_4]$ cluster of FeP can be reduced to the all-ferrous form at biologically relevant values of $E°$, which would make it available to perform two electron reduction of MoFeP per two ATPs hydrolyzed under biological conditions. Moreover, it explains why very different $E°$ have been found experimentally since different conditions may stabilize different protein conformations and thus cluster burial. Of course, this does not rule out $[Fe_4S_4]^{1+}$ in the biological pathway, which can perform one electron of MoFeP per two ATPs hydrolyzed and is thus less catalytically efficient, and both may be operable. These results also suggest that site-specific mutagenesis to stabilize a protein conformation with a more exposed cluster may be a means of bioengineering nitrogenase to be more efficient.

Acknowledgment

Computer resources are from the William G. McGowan Foundation, Georgetown University (Matrix), and the Environmental Molecular Sciences Laboratory at Pacific Northwest National Laboratory under the grants EMSL38793 and st39962 are gratefully acknowledged. The authors declare no competing financial interests.

References

1. Igarashi RY, Seefeldt LC (2003) Nitrogen fixation: the mechanism of the Mo-dependent nitrogenase. Crit Rev Biochem Mol Biol 38:351–384.
2. Watt GD, Reddy KRN (1994) Formation of an all ferrous Fe_4S_4 cluster in the iron protein component of *Azotobacter vinelandii* nitrogenase. J Inorg Biochem 53:281–294.
3. Rees DC, Howard JB (2000) Nitrogenase: standing at the crossroads. Curr Opin Chem Biol 4:559–566.
4. Angove HC, Yoo SJ, Burgess BK, Münck E (1997) Mössbauer and EPR evidence for an all-ferrous Fe_4S_4 cluster with S = 4 in the Fe protein of nitrogenase. J Am Chem Soc 119:8730–8731.
5. Guo M, Sulc F, Ribbe MW, Farmer PJ, Burgess BK (2002) Direct assessment of the reduction potential of the [4Fe-4S]1+/0 couple of the Fe protein from *Azotobacter vinelandii*. J Am Chem Soc 124:12100–12101.
6. Torres RA, Lovell T, Noodleman L, Case DA (2003) Density functional and reduction potential calculations of Fe_4S_4 clusters. J Am Chem Soc 125:1923–1936.
7. Lowery TJ, Wilson PE, Zhang B, Bunker J, Harrison RJ, Nyborg AC, Thiriot D, Watt GD (2006) Flavodoxin hydroquinone reduces *Azotobacter vinelandii* Fe

protein to the all-ferrous redox state with a $S = 0$ spin state. Proceedings of the National Academy of Science, USA 103:17131–17136.
8. Hollinger C, Pierik A, Reijerse E, Hagen W (1993) A spectroelectrochemical study of factor F430 nickel(II/I) from methanogenic bacteria in aqueous solution. J Am Chem Soc 115:5651–5656.
9. Chakrabarti M, Deng L, Holm RH, Munck E, Bominaar EL (2009) Mossbauer, electron paramagnetic resonance, and theoretical studies of a carbene-based all-ferrous Fe_4S_4 cluster: electronic origin and structural identification of the unique Spectroscopic Site. Inorg Chem 48:2735–2747.
10. Chakrabarti M, Muenck E, Bominaar EL (2011) Density functional theory study of an all ferrous 4Fe-4S cluster. Inorg Chem 50:4322–4326.
11. Jacobs D, Watt GD (2013) Nucleotide-assisted $[Fe_4S_4]$ redox state interconversions of the Azotobacter vinelandii Fe protein and their relevance to nitrogenase catalysis. Biochem 52:4791–4799.
12. Strop P, Takahara PM, Chiu H-J, Angove HC, Burgess BK, Rees DC (2001) Crystal structure of the all-ferrous $[4Fe\text{-}4S]^0$ form of the nitrogenase iron protein from Azotobacter vinelandii. Biochem 40:651–656.
13. Tezcan FA, Kaiser JT, Mustafi D, Walton MY, Howard JB, Rees DC (2005) Nitrogenase complexes: multiple docking sites for a nucleotide switch protein. Sci 309:1377–1380.
14. Tezcan FA, Kaiser JT, Howard JB, Rees DC (2015) Structural Evidence for Asymmetrical Nucleotide Interactions in Nitrogenase. J Am Chem Soc 137:146–149.
15. Perrin BS Jr., Ichiye T (2010) Fold versus sequence effects on the driving force for protein mediated electron transfer. Proteins: Struct, Funct, Bioinf 78:2798–2808.
16. Gerstein M, Lesk A, Chothia C (1994) Structural mechanisms for domain movements in proteins. Biochem 33: 6739–6749.
17. Perrin BS, Ichiye T (2013) Identifying Residues That Cause pH-Dependent Reduction Potentials. Biochem 52:3022–3024.
18. Perrin BS Jr., Ichiye T (2013) Characterizing the effects of the protein environment on the reduction potentials of metalloproteins. J Biol Inorg Chem 18: 103–110.
19. Niu S, Ichiye T (2011) Density functional theory calculations of redox properties of iron–sulphur protein analogues (invited review). Mol Simul 37:572–590.
20. Perrin BS, Jr. Niu S, Ichiye T (2013) Calculating standard reduction potentials of [4Fe–4S] proteins. J Comput Chem 34:576–582.
21. Zheng W, Doniach S (2003) A comparative study of motor-protein motions by using a simple elastic network model. Proc Natl Acad Sci USA 100:13253–13258.
22. Reiss H, Heller A (1985) The absolute potential of the standard hydrogen electrode: a new estimate. J Phys Chem 89:4207–4213.
23. Valiev M, Bylaska EJ, Govind N, Kowalski K, Straatsma TP, van Dam HJJ, Wang J, Nielplocha J, Aprà E, Windus TL, de Jong WA (2010) NWChem: a comprehensive and scalable open-source solution for large scale molecular simulations. Comput Phys Commun 181:1477–1489.
24. Becke AD (1993) Density-functional thermochemistry 3. The role of exact exchange. J Chem Phys 98:5648–5652. PMID: ISI:A1993KV99700048 {Medline}
25. Lee C, Yang W, Parr RG (1988) Development of the Colle-Salvetti correlation-energy formula into a functional of the electron density. Phys Rev B37:785–789.
26. Hehre WJ, Radom L, Schleyer PvR, Pople JA. 1986. Ab initio molecular orbital theory, John Wiley & Sons, New York.
27. Breneman CM, Wiberg KB (1990) Determining atom-centered monopoles from molecular electrostatic potentials. The need for high sampling density in formamide conformational analysis. J Comput Chem 11:361–373.
28. Jang S, Seefeldt L, Peters J (2000) Modulating the midpoint potential of the [4Fe-4S] cluster of the nitrogenase Fe protein. Biochem 39:641–648.
29. Dauter Z, Wilson KS, Sieker LC, Meyer J, Moulis JM (1997) Atomic resolution (0.94 Å) structure of Clostridium acidurici ferredoxin. Detailed geometry of [4Fe-4S] clusters in a protein. Biochem 36:16065–16073.
30. Berman HM, Westbrook J, Feng Z, Gilliland G, Bhat TN, Weissig H, Shindyalov IN, Bourne PE (2000) The protein data bank. Nucleic Acids Res 28:235–242.
31. Brooks BR, Bruccoleri RE, Olafson BD, States DJ, Swaminathan S, Karplus M (1983) CHARMM: a program for macromolecular energy, minimization, and dynamics calculations. J Comput Chem 4:187–217.
32. Baker NA, Sept D, Joseph S, Holst MJ, McCammon JA (2001) Electrostatics of nanosystems: application to microtubules and the ribosome. Proc Natl Acad Sci USA 98:10037–10041.
33. Connolly ML (1983) Solvent-accessible surfaces of proteins and nucleic acids. Science 221:709–713.
34. MacKerell A, Bashford D, Bellott M, Dunbrack R, Evanseck J, Field M, Fischer S, Gao J, Guo H, Ha S, Joseph-McCarthy D, Kuchnir L, Kuczera K, Lau F, Mattos C, Michnick S, Ngo T, Nguyen D, Prodhom B, Reiher W, Roux B, Schlenkrich M, Smith J, Stote R, Straub J, Watanabe M, Wiorkiewicz-Kuczera J, Yin D, Karplus M (1998) All-atom empirical potential for molecular modeling and dynamics studies of proteins. J Phys Chem B 102:3586–3616.
35. Zheng W, Brooks BR (2005) Probing the local dynamics of nucleotide-binding pocket coupled to the global dynamics: myosin versus kinesin. Biophys J 89:167–178.
36. Watt G, Wang Z, Knotts R (1986) Redox reactions of and nucleotide binding to the iron protein of *Azotobacter vinelandii*. Biochem 25:8156–8162.
37. Backes G, Davidson VL, Huitema F, Duine JA, Sanders-Loehr J (1991) Characterization of the tryptophan-derived quinone cofactor of methylamine dehydrogenase by Resonance Raman spectroscopy. Biochemistry 30:9201–9210.